Check for updates

JGR Oceans

RESEARCH ARTICLE

10.1029/2026JC024620

Drivers of Ocean pH Variation in Front of Dotson Ice Shelf, West Antarctica

Daisy D. Pickup[1], Dorothee C. E. Bakker[1], Karen J. Heywood[1], Emily M. Hammermeister[2,3], Yixi Zheng[1,4], Gareth A. Lee[1], Socratis Loucaides[3], David R. Munro[5,6], Bastien Y. Queste[7], Patricia L. Yager[8], and Rob A. Hall[1,9]

[1]Centre for Ocean and Atmospheric Sciences, School of Environmental Sciences, University of East Anglia, Norwich, UK, [2]School of Ocean and Earth Sciences, University of Southampton, Southampton, UK, [3]National Oceanography Centre, Southampton, UK, [4]Now at British Antarctic Survey, Cambridge, UK, [5]Cooperative Institute for Research in Environmental Sciences, University of Colorado, Boulder, CO, USA, [6]Global Monitoring Laboratory, National Oceanic and Atmospheric Administration, Boulder, CO, USA, [7]Department of Marine Sciences, University of Gothenburg, Gothenburg, Sweden, [8]Department of Marine Sciences, University of Georgia, Athens, GA, USA, [9]Now at Scottish Association for Marine Science, Oban, UK

Abstract The highly productive Amundsen Sea Polynya in West Antarctica is bounded in the south by rapidly-melting ice shelves, including the Dotson Ice Shelf (DIS). We present a high-resolution, full-depth pH data set within 10 km of DIS using a Lab-On-Chip (LOC) spectrophotometric pH sensor on an ocean glider. The LOC performs well with a 0.01 difference in pH between sensor measurements and discrete samples. Over 19 days in January–February 2022, the pH sensor captured the variability resulting from summertime biological and physical processes. At depth, modified Circumpolar Deep Water entering the DIS cavity exhibited a relatively low pH (7.91). The outflow had a higher average pH (7.94) as a result of dilution by glacial meltwater, but its pH was 0.01 lower than that of surrounding water at the same density. The Antarctic Coastal Current transported unventilated surface water with a low pH emerging from below fast ice east of Bear Island, westward to the eastern side of DIS. Net primary production increased pH in the upper 50 m in front of DIS, whilst temperature change was responsible for 5% of the change in pH. This study provides the first direct measurements of pH in the Amundsen Sea capable of deducing the impact of glacial meltwater on pH. It demonstrates the value, particularly in remote regions, of LOC pH sensors that have the longevity and stability to measure ocean pH without sensor drift.

Plain Language Summary Dotson Ice Shelf (DIS) is located in the Amundsen Sea, West Antarctica. We used a pH sensor attached to a profiling ocean glider to collect measurements close to DIS. Our observations show how pH in the upper ocean is influenced by the presence of a westward coastal current, biology and interactions with sea ice. Our results indicate that water entering underneath DIS has a relatively low pH and that water that gets modified below the ice shelf and exits on the west has a higher pH. We suggest that pH is increased by the addition of ice shelf meltwater. Our study highlights the variability of pH in remote, Antarctic coastal waters, both at the surface and at depth, and points to the importance and feasibility of increased ocean monitoring.

Key Points:

- High-resolution, full-depth ocean pH measurements were made in front of Dotson Ice Shelf (DIS) by a sensor on an ocean glider
- Dilution by glacial meltwater increased pH by 0.03 below DIS but the pH of the outflow was 0.01 lower than surrounding water
- Photosynthesis was a key process in increasing upper ocean pH, after water emerged from below sea ice

Supporting Information:

Supporting Information may be found in the online version of this article.

Correspondence to:

D. D. Pickup,
d.pickup@uea.ac.uk

Citation:

Pickup, D. D., Bakker, D. C. E., Heywood, K. J., Hammermeister, E. M., Zheng, Y., Lee, G. A., et al. (2026). Drivers of ocean pH variation in front of Dotson Ice Shelf, West Antarctica. *Journal of Geophysical Research: Oceans*, *131*, e2026JC024620. https://doi.org/10.1029/2026JC024620

Received 19 MAY 2026
Accepted 27 OCT 2026

Author Contributions:

Conceptualization: Daisy D. Pickup, Dorothee C. E. Bakker, Karen J. Heywood
Data curation: Daisy D. Pickup
Formal analysis: Daisy D. Pickup, Emily M. Hammermeister, David R. Munro
Funding acquisition: Karen J. Heywood, Patricia L. Yager, Rob A. Hall
Investigation: Daisy D. Pickup, Dorothee C. E. Bakker, Karen J. Heywood
Methodology: Daisy D. Pickup, Dorothee C. E. Bakker, Karen J. Heywood, Emily M. Hammermeister, Yixi Zheng, Gareth A. Lee, Socratis Loucaides, David R. Munro, Rob A. Hall
Resources: Socratis Loucaides

© 2026 The Author(s). Journal of Geophysical Research: Oceans published by Wiley Periodicals LLC on behalf of American Geophysical Union.
This is an open access article under the terms of the Creative Commons Attribution License, which permits use, distribution and reproduction in any medium, provided the original work is properly cited.

1. Introduction

The pH of the ocean is a measure of its hydrogen ion activity and provides an important indicator of changes in ocean carbonate chemistry. The modern global surface ocean is slightly alkaline, with a pH of approximately 8.1 (Jiang et al., 2019; Millero, 2007) and the ocean system has a buffering capability that maintains a stable pH. However, the global ocean absorbs 29% of anthropogenic carbon dioxide (CO_2) annually (Friedlingstein et al., 2026) and this large-scale uptake of anthropogenic CO_2 has led to a reduction in pH creating a phenomenon known as ocean acidification. The Southern Ocean is particularly sensitive to ocean acidification due to the region's low carbonate ion concentrations (Orr et al., 2005). To date, the most common type of sensor used to monitor pH in the Southern Ocean are ISFET (Ion-Sensitive Field-Effect Transistor) based sensors deployed on profiling floats (Johnson et al., 2017; Sarmiento et al., 2023). Few measurements are taken by these floats around the coast of Antarctica, as the floats do not typically survey in water shallower than 2,000 m. This leaves a gap in our knowledge of coastal pH variability. Coastal regions of Antarctica are especially important with regards to pH

21699291, 2026, 11, Downloaded from https://agupubs.onlinelibrary.wiley.com/doi/10.1029/2026JC024620 by British Antarctic Survey, Wiley Online Library on [13/11/2026]. See the Terms and Conditions (https://onlinelibrary.wiley.com/terms-and-conditions) on Wiley Online Library for rules of use; OA articles are governed by the applicable Creative Commons License

Supervision: Dorothee C. E. Bakker, Karen J. Heywood
Validation: Daisy D. Pickup, Emily M. Hammermeister, Bastien Y. Queste, Patricia L. Yager
Visualization: Daisy D. Pickup
Writing – original draft: Daisy D. Pickup
Writing – review & editing: Daisy D. Pickup, Dorothee C. E. Bakker, Karen J. Heywood, Emily M. Hammermeister, Yixi Zheng, Socratis Loucaides, David R. Munro, Bastien Y. Queste, Patricia L. Yager, Rob A. Hall

as they are key players in carbon uptake and sequestration. Thus, this data gap leads to a lack of understanding of how they will be affected by continuing ocean CO_2 uptake under climate change.

ISFET sensors are electrochemical pH sensors which are subject to drift over time and are typically corrected periodically on floats using comparisons with discrete samples taken at the classical reference depth of 1,500 m (Johnson et al., 2016, 2017). Field observations with these sensors show they can also take up to 10 days to stabilize when integrated on moving platforms (Hammermeister et al., 2026). These limitations highlight the need for alternative pH sensing approaches that can provide stable and high precision measurements when deployed on autonomous platforms in coastal environments. Lab-On-Chip (LOC) technology helps to bridge this gap. For pH, LOC sensors utilize the spectrophotometric approach (Yin et al., 2021), which has an excellent precision (<0.001) and is not subject to drift (Byrne & Breland, 1989; Clayton & Byrne, 1993). The robustness of LOC sensors over long term deployments (on the scale of 6 months) has been demonstrated in a harbor in Southampton, UK (Lucio et al., 2026). This makes them suitable to be integrated onto autonomous platforms which are typically deployed for weeks to months and are capable of surveying coastal polar environments. To date, a handful of studies have utilized a LOC pH sensor on an autonomous platform, on a profiling glider in the North Sea (Possenti et al., 2021) and on Autosub Long Range in Loch Ness (Yin et al., 2021) and the Celtic Sea (Hammermeister et al., 2025, 2026). The combination of the LOC pH sensor and profiling glider introduces the capability of surveying pH in remote coastal Antarctic regions to both a higher horizontal and vertical resolution than ship sampling alone.

Coastal polynyas are areas of open water surrounded by sea ice that play an important role in biogeochemical cycles on the Antarctic continental shelf, yet remain understudied because the persistent sea ice cover makes them difficult to access. The Amundsen Sea Polynya (ASP), off the coast of West Antarctica, is one of the most productive polynyas in the Southern Ocean (Arrigo & van Dijken, 2003). The polynya typically opens in December with little interannual variability (Macdonald et al., 2023). Phytoplankton blooms begin in December and lose intensity in mid-January (Arrigo et al., 2012). The eastern boundary of the ASP is a region of fast ice (Ohshima et al., 2016) and part of the southern boundary is the Dotson Ice Shelf (DIS) which is approximately 50 km wide (Figure 1a). The Dotson-Getz Trough sits within the polynya (Figure 1b) and acts as a conduit for warm salty water from offshore (Walker et al., 2013; Wåhlin et al., 2010) which causes basal melting when it intrudes under DIS (Wåhlin et al., 2010). Thus, the DIS region is subject to the addition of glacial meltwater from ice shelves. Modeling studies show that the majority of the meltwater-laden outflow travels westward (Nakayama et al., 2017; St-Laurent et al., 2017) with the Antarctic Coastal Current, a narrow current bounded by the coast. The remaining meltwater-laden is outflow carried in a northward flow within and around the Dotson-Getz Trough. This supplies necessary micronutrients to the ASP (Sherrell et al., 2015; St-Laurent et al., 2017; Twelves et al., 2021; Van Manen et al., 2022), enhancing its productivity. There is variability in these meltwater pathways, influenced by interannual variability in ice shelf melt rates (Kimura et al., 2017). Whilst the effects of glacial meltwater addition have not been studied near DIS, in East Antarctica the addition of glacial meltwater from basal melting of an ice shelf and glacier tongue has been shown to dilute DIC (dissolved inorganic carbon; Tamura et al., 2023) and reduce pCO_2 (partial pressure of CO_2; Kiuchi et al., 2021), respectively, in the meltwater-laden outflow. Both studies found that biological production had a greater influence on surface carbonate chemistry than meltwater dilution, highlighting the importance of considering the interplay between freshwater inputs and biological processes. This is particularly relevant to the ASP as a highly productive region, yet the link between dilution from glacial meltwater and primary production in the surface and subsurface has not yet been investigated.

Very few studies within the Amundsen Sea focus on carbonate chemistry, and even fewer specifically include measurements of pH. Efforts have been made to deduce the role of the polynya's phytoplankton bloom on the pCO_2 (Mu et al., 2014; Tortell et al., 2012) and pH (Mattsdotter Björk et al., 2014) in the surface ocean. The only published study with full-depth measurements of DIC and TA (total alkalinity) was carried out within the open polynya to investigate the efficiency of the biological carbon pump (Yager et al., 2016). This lack of in situ studies limits our understanding of how glacial melt is affecting carbonate chemistry in coastal waters in front of DIS.

Here, we use measurements from a LOC pH sensor on a profiling glider in the first deployment of its kind in the Southern Ocean. A small subset of pH measurements from this campaign have previously been reported by Pickup, Bakker, et al. (2025). The measurements presented in this study resolve the pH of the DIS inflow and outflow. By combining in situ pH observations with other measured biogeochemical variables, we also determine the mechanisms controlling pH variability in the upper ocean.

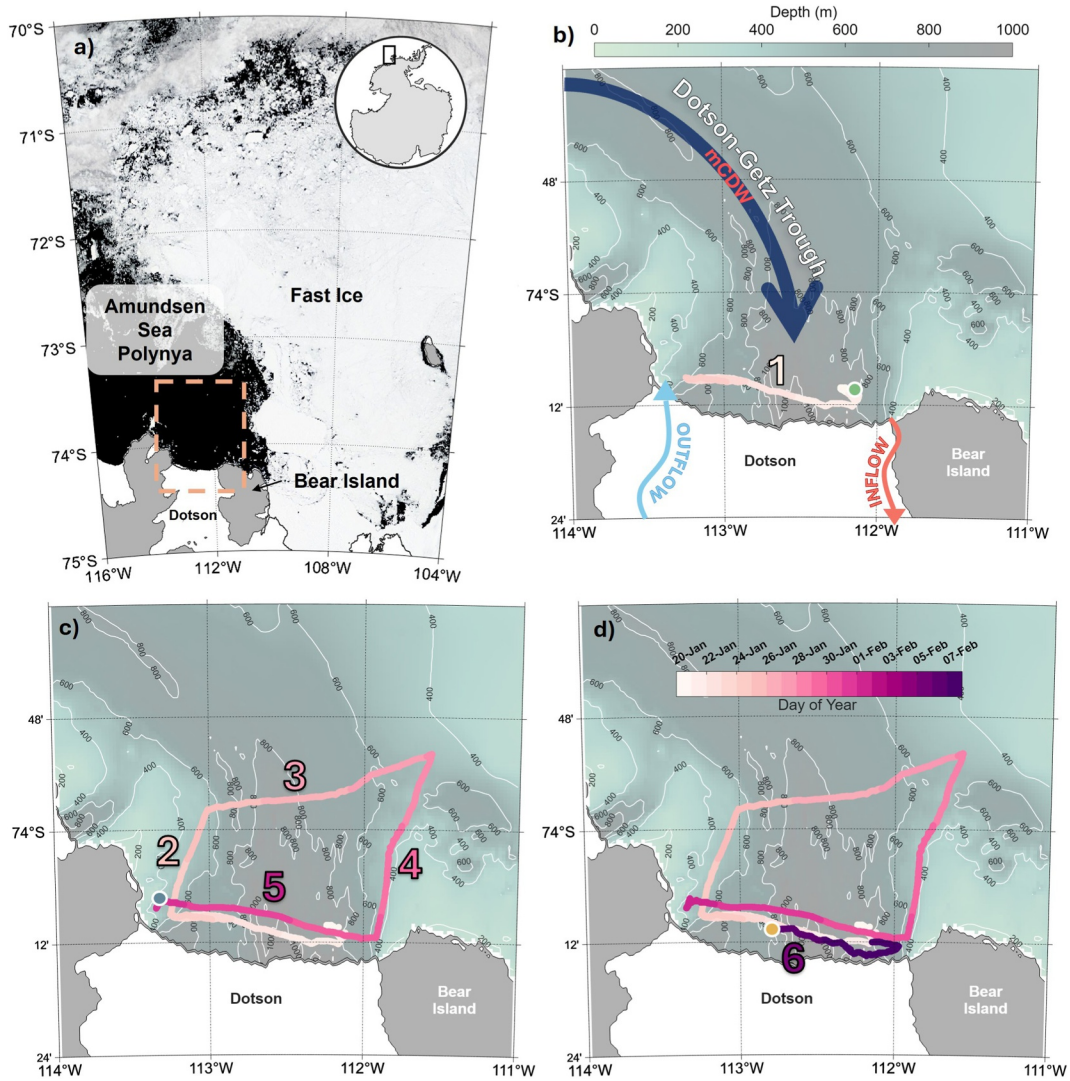


Figure 1. (a) The Amundsen Sea with sea ice imagery from Terra/MODIS on 21 January 2022. The orange box indicates the glider study region. Ice shelves are shown in white and land in gray. Inset: Map of Antarctica with the black box indicating the study location. (b) Map of study region depicted by the orange box area in (a) highlighting oceanographic features and the first leg of the glider mission. The green circle represents where the glider was deployed. (c) same as (b) but with legs 2-5 added. The blue circle depicts where the pH sensor was temporarily switched off. (d) same as (c) but with leg 6 added. The yellow circle shows where the glider was redeployed after being temporarily recovered. Numbers indicate glider legs used throughout the text and legs are colored by date. Bathymetry with contours (in m) is from BedMachine v3 (Morlighem, 2022).

2. Data and Methods

2.1. Lab-On-Chip pH Sensor

The LOC pH sensor was supplied by the National Oceanography Centre (Southampton, UK). It determines pH spectrophotometrically, using purified meta-cresol purple (mCP) as an indicator dye (Yin et al., 2021) and does not require a correction for drift unlike electrochemical pH sensors. The sensor is a microfluidic platform that contains a built-in optical system consisting of two LEDs (wavelengths 435 and 590 nm) for light emission and a photodiode detector. An internal thermistor records the temperature within the sensor during measurement. Upon addition of the mCP, absorption of the sample is measured at both wavelengths and used to calculate the sample pH. The sensor itself is 125 mm × 195 mm and weighs 0.85 kg in water, making it suitable for integrating into autonomous platforms. Further information on the sensor is provided by Yin et al. (2021).

21699291, 2026, 11, Downloaded from https://agupubs.onlinelibrary.wiley.com/doi/10.1029/2026JC024620 by British Antarctic Survey, Wiley Online Library on [13/11/2026]. See the Terms and Conditions (https://onlinelibrary.wiley.com/terms-and-conditions) on Wiley Online Library for rules of use; OA articles are governed by the applicable Creative Commons License

21699291, 2026, 11, Downloaded from https://agupubs.onlinelibrary.wiley.com/doi/10.1029/2026JC024620 by British Antarctic Survey, Wiley Online Library on [13/11/2026]. See the Terms and Conditions (https://onlinelibrary.wiley.com/terms-and-conditions) on Wiley Online Library for rules of use; OA articles are governed by the applicable Creative Commons License

The LOC sensor was attached to University of East Anglia (UEA) Seaglider 579 (SG579). During sampling, a small volume of water is flushed twice throughout the tubing before a measurement is taken, which contributes to the 8 min sampling interval. The sensor intake tube withdraws water over a 30-s period, meaning pH measurements are associated with the depth range covered by the glider over that 30-s period. The glider was programmed so that the ascent was slower (vertical velocity of 0.09 m s^{-1}) than the descent (0.15 m s^{-1}), yielding higher vertical-resolution pH values on the ascent (approximately 55 vs. 95 m for the descent) with the withdrawal depth range covering approximately 3 m. Only pH measurements associated with glider ascent are included in this study.

For converting raw absorption data to in situ pH measurements, coincident in situ temperature and salinity from SG579 were required. Mean temperature and salinity were calculated over the 30 s coinciding with a sample withdrawal. The raw pH values were then corrected for temperature differences between the sensor's thermistor and in situ temperature ($T_{\text{thermistor}} - T_{\text{insitu}} = 2.94 \pm 1.00$°C, Figure S1a in Supporting Information S1), that arose from waste heat from the pH sensor's electronics, following Yin et al. (2021) using the equation by Millero (1995):

$$pH = pH_{\text{raw}} - 0.01582 \times (T_{\text{thermistor}} - T_{\text{insitu}}) \quad (1)$$

where pH_{raw} is the uncorrected pH (Figure S1b in Supporting Information S1), $T_{\text{thermistor}}$ is the temperature recorded by the LOC sensor's internal thermistor and T_{insitu} is the ambient water temperature measured by the Seabird CT sensor on the glider, averaged over 30 s. Final pH values (Figure S1c in Supporting Information S1) are reported at in situ temperature, salinity and pressure and on the total hydrogen scale.

The LOC pH sensor is associated with a precision of 0.001 and an accuracy of 0.003 ± 0.022 as reported by Yin et al. (2021). Values of pH in the most stable regional water mass, mCDW (modified Circumpolar Deep Water, see Section 3.1 for water mass discussion) from the LOC sensor ($n = 376$, Figure S2a in Supporting Information S1) compared well with pH calculated from discrete samples of DIC and TA ($n = 16$, Figure S2a in Supporting Information S1), giving a 0.01 ± 0.003 difference which we report as the uncertainty of the LOC sensor in this study (Table S1 and Figure S2b in Supporting Information S1). The 500 mL seawater samples used for DIC and TA were collected from stations within 50 km and a 3 week period of the glider measurements. Upon collection, the samples were stored in borosilicate bottles, fixed with mercuric chloride and sealed according to Standard Operating Procedure (SOP) 1 of Dickson et al. (2007). Samples for DIC were analyzed at the University of Georgia using a Single Operator Multi-parameter Metabolic Analyzer (SOMMA) attached to a UIC CM5011 CO_2 coulometer. Precision based on duplicate samples (repeatability) was 0.90 μmol kg^{-1}. Samples for TA were analyzed at the University of East Anglia using a VINDTA 3C system (Versatile INstrument for the Determination of Total dissolved inorganic carbon and titration Alkalinity). The potentiometric titration system for the determination of TA follows SOP 3b of Dickson et al. (2007). Repeatability precision was 1.82 μmol kg^{-1}. From the discrete values, pH on the total hydrogen scale was calculated using CO2SYS (Lewis et al., 1998; Sharp et al., 2023) and was associated with an uncertainty of 0.01 propagated from the DIC and TA repeatability precision and the parameterizations used (using the CO2SYS function *errors.m* (Orr et al., 2018; Sharp et al., 2023)). The parameterizations used throughout the system calculations are listed in Table S2 of the Supporting Information S1 and the various sources of error on pH are listed in Table S1 of the Supporting Information S1.

Due to the temporal resolution of the LOC sensor (every 8 min), no measurements were taken shallower than 5 m and only 10 measurements were taken shallower than 20 m depth. Therefore, we define measurements in the top 50 m of the water column as the upper ocean to provide a consistent basis for discussion. These measurements are all above the WW (Winter Water, see Section 3.1 for water mass discussion) core which is defined as the temperature minimum.

2.2. Other Glider Sensors

The glider was equipped with integrated sensors measuring conductivity and temperature (Seabird CT sail), and chlorophyll fluorescence and optical backscatter (WetLabs ECO puck BB2FLVMT), that took measurements every 5 s. Corrections for the thermal lag of the un-pumped conductivity cell that produces artificial salinity

21699291, 2026, 11, Downloaded from https://agupubs.onlinelibrary.wiley.com/doi/10.1029/2026JC024620 by British Antarctic Survey, Wiley Online Library on [13/11/2026]. See the Terms and Conditions (https://onlinelibrary.wiley.com/terms-and-conditions) on Wiley Online Library for rules of use; OA articles are governed by the applicable Creative Commons License

spikes were made following Garau et al. (2011). Conservative temperature (Θ) and absolute salinity (S_A) were calculated from in situ temperature and conductivity using TEOS-10 (McDougall et al., 2010).

Chlorophyll fluorescence concentrations (mg m^{-3}) were calculated from chlorophyll fluorescence counts and validated against the chlorophyll fluorescence sensor (Figure S2a in Supporting Information S1) mounted on the ship's conductivity-temperature-depth (CTD) rosette which had been corrected against filtered discrete samples. Values were then corrected for non-photochemical quenching using particulate backscatter. Particulate backscatter was calculated from the raw optical backscatter observations using a centroid angle of 124° and a wavelength of 700 nm (Green et al., 2014) and subtracting the water scattering component (Zhang et al., 2009). The quenching depth was determined to be 10 m following the method of Thomalla et al. (2018) after separating the measurements into daylight and darkness. The fluorescence-to-particulate backscatter ratio in the upper 10 m during darkness hours was used to correct the chlorophyll fluorescence values measured in the upper 10 m during daylight hours (Figure S2b in Supporting Information S1).

2.3. Glider Mission

SG579 was deployed in open water in the coastal southern Amundsen Sea on 20 January 2022 at 74.17°S 112.16°W, approximately 10 km north of the DIS front (Figure 1b). SG579 completed 146 dives to 1,000 m depth, or a few meters above the seabed, whichever was shallower, before pH data collection ceased on 8 February 2022 at 74.20°S 112.19°W. Within this 19-day period the glider surveyed a closed box, split into legs 1–6 (Figures 1b–1d). Legs 1, 5 and 6 surveyed the front of DIS with leg 5 being the longest and covering 44 km. Leg 3 (46 km) crossed the Dotson-Getz Trough further north, parallel to the ice shelf front. Northward leg 2 (22 km) closed the box in the west and southward leg 4 (38 km) closed the box in the east. The glider was temporarily recovered between legs 5 and 6 for emptying the LOC sensor waste bags and downloading data.

2.4. Shipborne Data

Surface water properties were measured using the underway seawater intake system at 5 m depth on board the *R/V Nathaniel B. Palmer*. The pCO_2 system continuously measured surface water pCO_2 using a showerhead equilibrator and a non-dispersive infrared CO_2 gas analyzer (Sweeney et al., 2023). The pCO_2 measurements have a reported accuracy of ±2 µatm. Underway oxygen was measured by an Aanderaa 4835 Oxygen Optode which has a reported accuracy of <4 µmol L^{-1}. Underway O_2 measurements were calibrated against measurements of O_2 from the sensor on the ship's CTD rosette (SBE 43, which was calibrated against discrete samples) made at 5 m depth which gave an offset of 57 µmol L^{-1}; this offset was subtracted from the underway sensor measurements.

Ocean current velocities were measured using a 38 Hz Ocean Surveyor (OS38) shipboard Acoustic Doppler Current Profiler (SADCP) and processed following Hummon and Firing (2003) with a temporal resolution of 5 min and a vertical resolution of 24 m. No detiding was applied to the measurements as tidal currents in this region are less than 0.03 m s^{-1} in both a barotropic tide model (Circum-Antarctic Tidal Simulation Model CATS2008b (Padman et al., 2002)) and moored current velocity measurements in the central Amundsen Sea (Wåhlin et al., 2010). This is smaller than most non-tidal currents in the region; for example, the Antarctic Coastal Current has maximum speeds around 0.4 m s^{-1} in the upper 70 m (Kim et al., 2016). To capture the coastal current, velocities from OS38 were vertically-averaged from the uppermost bin (centered at 47 m) to 191 m depth.

2.5. Glacial Meltwater Calculation

We calculate glacial meltwater (GMW) content for legs 1, 5, and 6, following the composite tracer method (Jenkins, 1999) using Θ and S_A measurements from SG579. We use three water masses: mCDW, WW and glacial meltwater. The endpoint of mCDW ($\Theta = 0.5$°C, $S_A = 34.73$ g kg^{-1}, Figure 2) is consistent with previous observations in the region (Ha et al., 2014; Miles et al., 2016; Wåhlin et al., 2010; Yang et al., 2022) and is the same as the endpoint used by Wåhlin et al. (2024). The endpoint of WW ($\Theta = -1.86$°C, $S_A = 34.25$ g kg^{-1}, Figure 2) is derived from our glider observations and extrapolation to the freezing line following Biddle et al. (2019) to determine the endpoint for pure WW. WW with these properties was seen inside the DIS cavity (Wåhlin et al., 2024). The endpoint of glacial meltwater ($\Theta = -90.8$°C, $S_A = 0$ g kg^{-1}) is the same as that used by Biddle et al. (2019) and Wåhlin et al. (2024) for the Amundsen Sea. The glacial meltwater content $(\varphi_{\text{meltwater}})$ is derived following Equation 2:

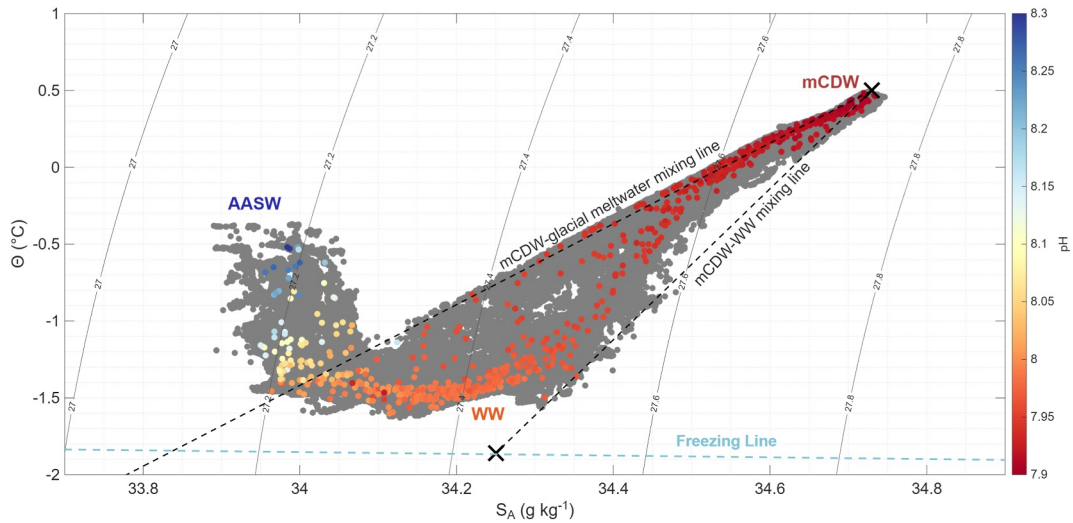


Figure 2. Θ and S_A for glider legs 1,5 and 6 colored by pH. Gray data points are where there is no corresponding pH measurement. The contours represent potential density (kg m^{-3}) and the different water masses are labeled. The crosses depict the relevant end-members and the freezing line (blue) was calculated using (McDougall et al., 2010). The black dashed lines represent mixing between different water masses.

$$\varphi_{\text{meltwater}} = \frac{\Theta_{\text{observed}} - \Theta_{\text{mCDW}} - \frac{(S_{\text{Aobserved}} - S_{\text{AmCDW}}) \times (\Theta_{\text{WW}} - \Theta_{\text{mCDW}})}{(S_{\text{AWW}} - S_{\text{AmCDW}})}}{\Theta_{\text{meltwater}} - \Theta_{\text{mCDW}} - \frac{(S_{\text{Ameltwater}} - S_{\text{AmCDW}}) \times (\Theta_{\text{WW}} - \Theta_{\text{mCDW}})}{(S_{\text{AWW}} - S_{\text{AmCDW}})}} \quad (2)$$

The glacial meltwater content is not calculated for measurements above the WW temperature-minimum layer where air-sea interactions further modify water properties, as the calculation assumes that the water temperature and salinity are conservative.

3. Results

3.1. pH in Different Water Masses

The deepest water mass observed by the glider is mCDW (Figure 2), derived from CDW that has traveled on shelf and become modified through interaction with surrounding water (Arneborg et al., 2012; Assmann et al., 2013; Wåhlin et al., 2013) and is associated with the lowest pH (between 7.90 and 7.92). This is consistent with isolation of mCDW (and its predecessor water masses) from the atmosphere and consequent accumulation of DIC. The warmest and saltiest mCDW ($\Theta > 0.3$°C, $S_A > 34.7$ g kg^{-1}) was seen at depths greater than 600 m in legs 1, 3, 5 and 6 in the deepest part of the Dotson-Getz Trough (Figures S4a and S4b in Supporting Information S1) and is associated with the lowest pH (Figure S4c in Supporting Information S1). These depth ranges and properties are consistent with previous studies in the Dotson region (Miles et al., 2016; Randall-Goodwin et al., 2015; Van Manen et al., 2022; Yang et al., 2022).

Above the mCDW is Winter Water (WW, Figure 2), the remnant of the previous winter surface layer. WW is located between 60 and 132 m depth (Figures S4a and S4b in Supporting Information S1) with similar properties to the WW observed by Randall-Goodwin et al. (2015). WW has a higher pH than mCDW by 0.05–0.10 (Figure S4d in Supporting Information S1). This difference may partly reflect the more recent interaction of WW with the atmosphere prior to ice formation and a small contribution of photosynthesis as concentrations of chlorophyll fluorescence within the WW are slightly above 0 mg m^{-3} (Figure S4c in Supporting Information S1).

The surfacemost water mass is Antarctic Surface Water (AASW, Figure 2), which is WW that has been modified by warming and ice melt. In AASW, located above the WW temperature minimum, pH is variable with a range of 7.97–8.30 (Figure 2). This water mass exhibits the highest pH because it is subject to biological CO_2 uptake during photosynthesis in summer. In the upper ocean, pH is more variable than at depth, with a standard deviation of 0.09 compared with a standard deviation of 0.05 below 50 m to the sea floor. Upper ocean pH is higher toward

21699291, 2026, 11, Downloaded from https://agupubs.onlinelibrary.wiley.com/doi/10.1029/2026JC024620 by British Antarctic Survey, Wiley Online Library on [13/11/2026]. See the Terms and Conditions (https://onlinelibrary.wiley.com/terms-and-conditions) on Wiley Online Library for rules of use; OA articles are governed by the applicable Creative Commons License

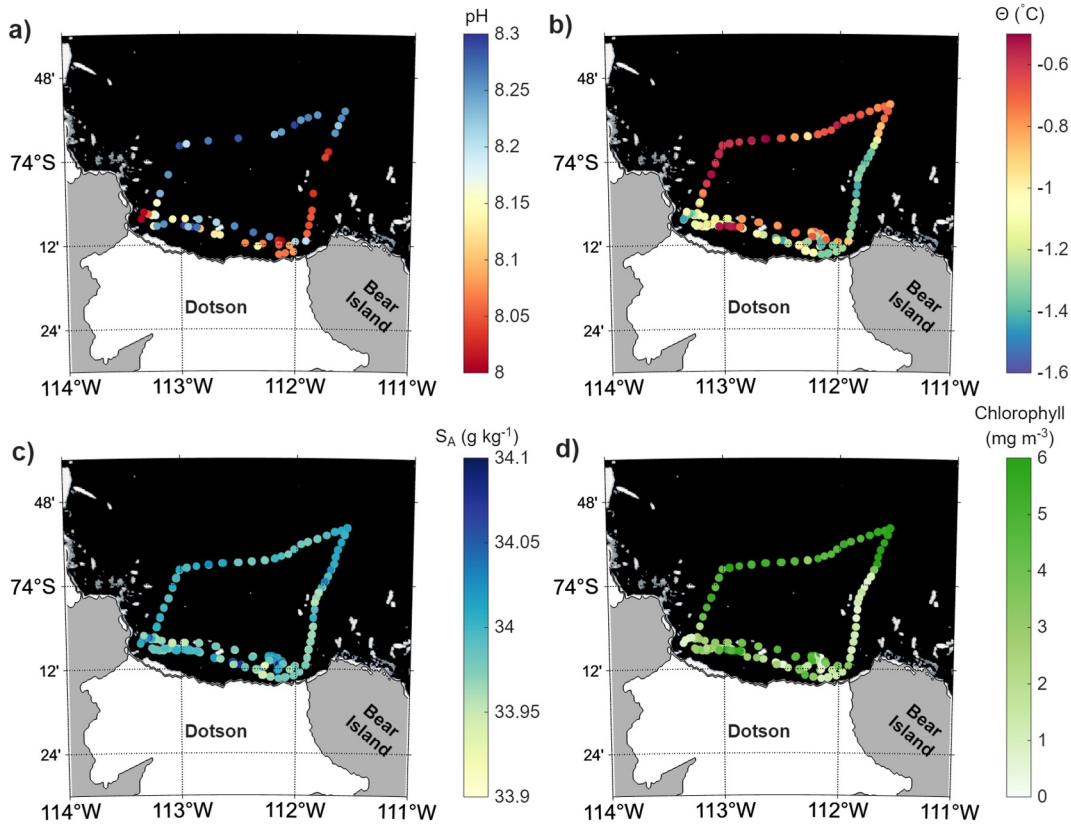


Figure 3. Upper ocean (<50 m) values for SG579 colored by (a) pH, (b) Θ, (c) S_A and (d) chlorophyll fluorescence. Sea ice imagery from Terra/MODIS on 21 January 2022.

the center of the DIS front than at the eastern and western ends with a maximum of 8.38 at 30 m depth and 112.4°W (Figure 3a). There is also a segment of measurements with a low pH (0.1 lower than the surface average of 8.16) south of 74°S on leg 4 (Figure 3a). This coincides with a lower Θ, S_A and chlorophyll fluorescence (Figures 3b–3d).

A cold subsurface lens was observed on leg 3 (Figure S4a in Supporting Information S1) in the Dotson-Getz Trough, deeper in the water column than the WW layer (240–400 m), as described by Pickup, Bakker, et al. (2025). The core of the lens has a Θ less than −1.73°C and S_A ranges between 34.25 and 34.35 g kg^{-1}, saltier than the WW described above (Figure S4a and S4b in Supporting Information S1). This cold water has slightly lower pH (8.00) than the overlying WW (8.02, Figure S4d in Supporting Information S1). Whilst the Θ and S_A properties may resemble supercooled Ice Shelf Water, glacial meltwater-enriched water in the Amundsen and Bellingshausen Seas is relatively warm because it is made up of mostly warm mCDW with a small addition of cold, fresh glacial meltwater (Jenkins, 1999). The observed cold and salty water mass is hypothesized to arise as a result of wintertime surface cooling and brine rejection in areas with intense sea ice formation, forming in shallower areas then spilling off into the deeper trough (Pickup, Bakker, et al., 2025).

3.2. DIS Inflow and Outflow Properties

The glider surveyed the region immediately north of the DIS ice front in three legs (1, 5 and 6 in Figure 1). The measurements made during these are shown in Figure 4, alongside an SADCP meridional current velocity transect along the ice shelf front. The SADCP measurements did not extend to the seabed, but captured a southward velocity increasing to 0.25 m s^{-1} at about 600 m depth on the eastern side of DIS (112°W) which is indicative of the inflow under DIS and agrees with previous observations (Miles et al., 2016; Van Manen et al., 2022; Wåhlin et al., 2010; Yang et al., 2022). These also correspond to water with the properties of mCDW (Figures 2 and 3b

21699291, 2026, 11, Downloaded from https://agupubs.onlinelibrary.wiley.com/doi/10.1029/2026JC024620 by British Antarctic Survey, Wiley Online Library on [13/11/2026]. See the Terms and Conditions (https://onlinelibrary.wiley.com/terms-and-conditions) on Wiley Online Library for rules of use; OA articles are governed by the applicable Creative Commons License

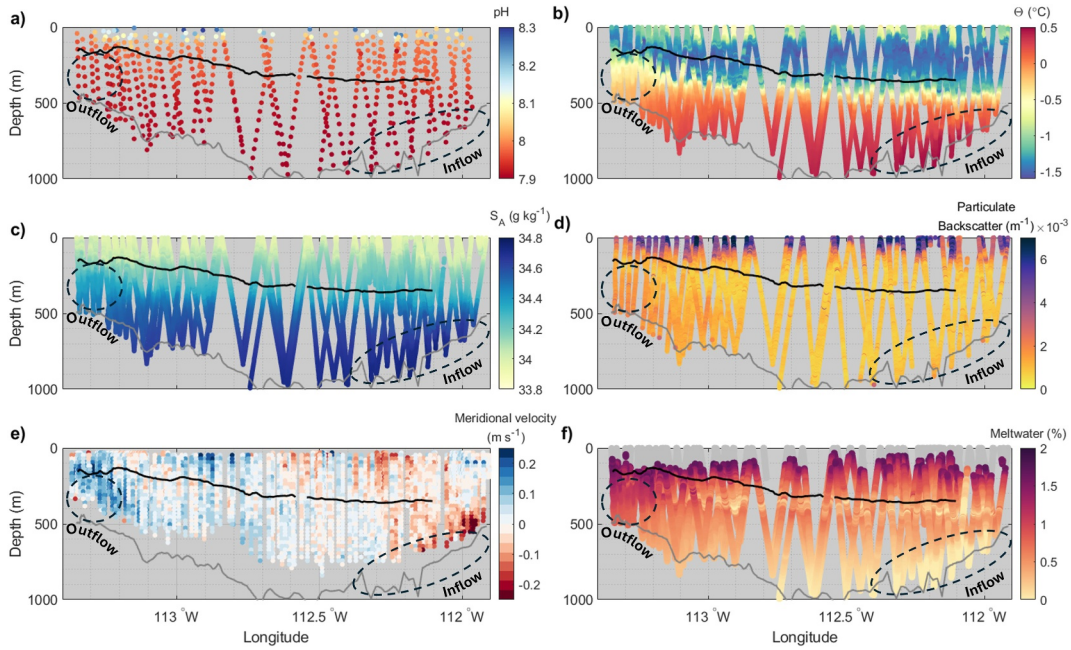


Figure 4. Measurements in front of DIS from (a)–(d) glider legs 1, 5 and 6, (e) shipboard SADCP and (f) glacial meltwater calculation based on glider measurements. (a) pH, (b) Θ, (c) S_A, (d) optical backscatter at 700 nm, (e) meridional velocity and (f) calculated glacial meltwater percentage. Ellipses with black dashes indicate the general locations of the outflow from below DIS (west) and the inflow to below DIS (east). The thick black line represents the base of the ice shelf detected by an autonomous underwater vehicle (Wåhlin et al., 2024) and the gray line is bathymetry from BedMachine v3 (Morlighem, 2022).

and 3c). In the inflow, seawater pH has a mean of 7.91 ± 0.004 (Figure 4a) and negligible mean glacial meltwater content (Figure 4f).

The western side of the ice shelf between 113.35°W and 113.20°W exhibits an elevated 700 nm particulate backscatter signal in our glider observations at depths between 200 and 400 m (Figure 4e) suggesting the presence of glacial debris. Consistent with this signal is a northward current that peaks at 0.2 m s^{-1} on the western side of DIS (Figure 4f). A similar signal was seen in vertical microstructure profile measurements from the same campaign that identified an outflow with a core at approximately 250 m and current speeds of 0.15 m s^{-1} (Dotto et al., 2025). The agreement among independent observations of temperature, salinity, backscatter, currents and turbulence provides confidence that this is the glacial meltwater outflow location. Furthermore, an enhanced glacial meltwater contribution is exhibited within the waters identified as the outflow (Figure 4f), between 200 and 423 m depth. Here the glacial meltwater content reaches as high as 1.6% with a mean of 1.000% ± 0.001%. Following the observations, the meltwater-laden outflow is characterized in this study as Θ between −1.35 and −0.30°C and S_A between 34.26 and 34.45 g kg^{-1}. These temperature and salinity properties compare well with previous studies (Miles et al., 2016; Van Manen et al., 2022; Yang et al., 2022). The outflow is a mixture of the inflow (small component of WW and large component of mCDW) with additional meltwater from DIS, so it is warmer and saltier than the ambient water at these depths and densities, and cooler and fresher than the mCDW inflow (Figures 4b and 4c). The mean pH in the meltwater-laden outflow is 7.94 ± 0.006, which is 0.03 greater than in the inflow.

3.3. The Effect of Dilution on pH

To assess whether dilution by glacial meltwater is the primary process responsible for the difference in pH between the inflow and meltwater-laden outflow, we calculate the expected pH as a result of the mixing between the inflow and pure glacial meltwater. We use the percentage contribution of each water mass to determine what DIC and TA should be in the outflow after the inflow has mixed with the glacial meltwater. We then use these values to estimate the expected pH in the outflow using CO2SYS (Lewis et al., 1998; Sharp et al., 2023).

21699291, 2026, 11, Downloaded from https://agupubs.onlinelibrary.wiley.com/doi/10.1029/2026JC024620 by British Antarctic Survey, Wiley Online Library on [13/11/2026]. See the Terms and Conditions (https://onlinelibrary.wiley.com/terms-and-conditions) on Wiley Online Library for rules of use; OA articles are governed by the applicable Creative Commons License

21699291, 2026, 11, Downloaded from https://agupubs.onlinelibrary.wiley.com/doi/10.1029/2026JC024620 by British Antarctic Survey, Wiley Online Library on [13/11/2026]. See the Terms and Conditions (https://onlinelibrary.wiley.com/terms-and-conditions) on Wiley Online Library for rules of use; OA articles are governed by the applicable Creative Commons License

All of the input values for the mixing equations are listed in Table S3 of the Supporting Information S1. Discrete water samples from this campaign were used to determine the mean DIC and TA concentrations in the inflow. As CO2SYS requires in situ temperature and practical salinity (hereafter referred to as salinity) as inputs rather than Θ and S_A, these will be referred to in this section. They were deduced from the glider measurements as the average for each water mass. Nutrient end-members for mCDW and WW, required for the CO2SYS calculation, are taken from Yager et al. (2016).

The percentage of each water mass present was calculated using Equation 3. In the outflow, the mean glacial meltwater, WW and mCDW percentages were 1.04%, 3.33% and 95.63%, respectively. We assume that the WW-to-mCDW ratio remains constant between the inflow and outflow, that is, unchanged by the addition of 1.04% of glacial meltwater to the water column. Under this assumption, any outflow property can be expressed as a weighted mixture of the three water mass end-member properties:

$$\left(95.63 \times p_{m\mathrm{CDW}}\right) + \left(1.04 \times p_{\mathrm{GMW}}\right) + \left(3.33 \times p_{\mathrm{WW}}\right) \quad (3)$$

where p represents properties and is substituted for the properties of each variable input for each water mass (Table S3 in Supporting Information S1). We check the validity of these water mass percentages using practical salinity (as a conservative variable) assuming a salinity of 0 in GMW, 33.99 in WW and 34.56 in mCDW. The output of 34.18 is close to the observed outflow average of 34.19 (Table S3 in Supporting Information S1), suggesting that the percentages in our mixing equations are robust.

Using the percentage contributions of each water mass, observed values for mCDW and WW, and estimations of 0 μmol kg^{-1} for GMW (Table S3 in Supporting Information S1), we estimate values of DIC of 2,236 μmol kg^{-1}, TA of 2,318 μmol kg^{-1} and pH of 7.93 in the outflow. The observed values in the outflow are also reported in Table S3 of the Supporting Information S1. Observed DIC in the outflow is 2,210 μmol kg^{-1}, which is slightly lower than our estimated value. A comparison for TA in the outflow cannot be made as the samples are yet to be analyzed.

There are uncertainties associated with this estimation, as we assume DIC and TA are 0 μmol kg^{-1} in glacial meltwater. In reality, there will be a small amount of both as a result of precipitation and mineral weathering. For example, at the West Antarctic Peninsula, Legge et al. (2017) deduced meteoric DIC and TA end-members from ice samples as 16 ± 5 μmol kg^{-1} and 100 ± 5 μmol kg^{-1}, respectively. Yet, no measurements of DIC and TA in ice exist for the Amundsen Sea region. It is not possible to quantify these uncertainties on our pH estimation, but they are important to consider when interpreting the results. The estimated pH calculated from DIC and TA is associated with an uncertainty of 0.01 (Section 2.1, Table S1 in Supporting Information S1).

4. Discussion

4.1. How the Circulation Under Dotson Alters pH

This study presents the first direct measurements of pH at both the inflow (east) and outflow (west) of the DIS cavity. Our findings for glacial meltwater content on the western side of the transect agree with those of Yang et al. (2022) who observed meltwater between 272 and 540 m depth in the same location, and those of Miles et al. (2016) who saw it between 100 and 500 m depth. Their calculated glacial meltwater contents of approximately 0.75% and 1.2%, respectively, compare well with our finding of 1.04% (Figure 4f). Both studies used the method of Jenkins (1999) to calculate their meltwater content with Miles et al. (2016) also incorporating O_2 concentration. Their choices in endpoints varied slightly to each other and to those used in our study which is likely due to interannual variability of water masses (Jenkins et al., 2018; Kim et al., 2021; Zheng et al., 2021). This should be considered when comparing between studies as it will lead to slight differences in the deduced meltwater concentration (Table S4 in Supporting Information S1). The chosen end-members for this study are consistent with Jenkins et al. (2018) who collated temperature and salinity data from a decade of observations in front of DIS.

Within the outflow, the observed pH (7.94) differs by 0.01 from the estimated pH (7.93), which is within the propagated uncertainty of 0.01 pH units associated with the DIC and TA repeatability (Table S1 in Supporting Information S1). We therefore consider the estimated and observed pH values to be consistent and attribute the

21699291, 2026, 11, Downloaded from https://agupubs.onlinelibrary.wiley.com/doi/10.1029/2026JC024620 by British Antarctic Survey, Wiley Online Library on [13/11/2026]. See the Terms and Conditions (https://onlinelibrary.wiley.com/terms-and-conditions) on Wiley Online Library for rules of use; OA articles are governed by the applicable Creative Commons License

0.03 increase in pH from the inflow to the outflow (east to west) to changes in carbonate chemistry resulting from mixing between the inflow and glacial meltwater under DIS. The low DIC concentration of glacial meltwater is the result of the low CO_2 (and DIC) concentration of precipitation (mainly as snow) in unpolluted, clean air. Subsequently, the glacial meltwater that mixes with the inflow lowers the DIC concentration such that the meltwater-laden outflow has a lower DIC concentration than the inflow, which is predominantly mCDW. This reveals the role of glacial meltwater input on pH, and by proxy on other carbonate chemistry variables, in the Amundsen Sea. Changes to other carbonate chemistry variables in meltwater outflows in East Antarctica have also shown evidence of modification by glacial meltwater dilution (Kiuchi et al., 2021).

Whilst there is an increase in pH relative to mCDW, the pH of the meltwater-laden outflow is 0.01 lower relative to the pH of ambient seawater. This reflects its substantial mCDW component. It suggests that ice shelf outflows in warm shelf regimes may act as a pathway for redistributing relatively low pH waters higher up within the water column through a mechanism known as the glacial meltwater pump. The implications of this are dependent on the fate of the meltwater outflow but likely to become more prominent as the melt rate in West Antarctica increases throughout the twenty-first century (Naughten et al., 2023). Modeling of glacial meltwater pathways suggest that the majority of the meltwater from DIS is transported west with the coastal current and some circulates within the Dotson-Getz Trough (Nakayama et al., 2017; St-Laurent et al., 2017). The observations presented here demonstrate that glacial meltwater from basal melt can modify subsurface carbonate chemistry immediately downstream of DIS through the glacial meltwater pump. However, our observations do not constrain the extent to which this signal persists, which depends on the pathways and spatial distribution of meltwater. Southern Ocean pH is changing on large spatial scales, with observed trends being attributed to changes in ocean circulation and increased anthropogenic CO_2 (Mazloff et al., 2023). Whether processes associated with basal melt contribute to these larger scale changes depends on how far the meltwater signals are transported beyond the continental shelf. Better understanding of the meltwater pathways and observations along them are therefore needed to link our study to larger scales.

The processes observed at DIS may also be present at other high melt rate ice shelves which are prominent in the Amundsen and Bellingshausen Seas. The extent to which surface and subsurface waters are affected by glacial meltwater, however, is linked to the outflow depth and settling depth of the meltwater laden plume. Observations at the nearby Pine Island Glacier demonstrate that meltwater can be exported laterally and settle at depth (Naveira Garabato et al., 2017) and further work suggests that the depth at which meltwater settles is seasonally dependent, reaching shallower depths during winter meaning nutrients are within the euphotic zone once the spring bloom begins (Zheng et al., 2021). In contrast, ice shelves in colder regions such as the Ross and Weddell seas may experience a weaker meltwater pump effect as lower basal melt rates result in smaller glacial inputs (Reese et al., 2018). Furthermore, a study by Dinniman et al. (2020) highlights that iron from the meltwater pump is only the dominant source in regions with lots of warm CDW suggesting impacts will be more prominent in regions with warm cavity ice shelves, like the Amundsen Sea.

4.2. Relationships Between Upper Ocean pH and Other Variables

To understand the drivers of pH variation in the upper ocean (shallower than 50 m), we investigate its relationship with Θ, S_A and chlorophyll fluorescence. Note that these three variables do not provide information on the effect of air-sea CO_2 exchange on pH which will also contribute to variability. S_A explains little of the observed pH variability (Figure 5a). This may reflect the seasonal timings of our observations, as seasonal sea ice melt had largely occurred months before our February observations, especially as the area in front of DIS is one of the first areas of the ASP to open up in spring (Macdonald et al., 2023). Consequently, the influence of recent sea ice melt and associated freshening on surface carbonate chemistry may have been limited during our observations.

The similar, high coefficients of determination for pH and Θ (Figure 5b) and for pH and chlorophyll fluorescence (Figure 5c) suggest that temperature and chlorophyll fluorescence co-vary, confirmed by the coefficient of determination for chlorophyll and temperature of 0.9 (not shown). When pH is standardized to a constant temperature (using Equation 1), the coefficient with Θ changes only slightly to 0.89, indicating temperature is not the primary driver of pH variability. The relationship between temperature and pH is a 0.0158 pH change for every 1°C change (Millero, 1995). Given the range in pH (8–8.3) and range in Θ (−1.45°C to −0.50°C), temperature only accounts for approximately 5% of the pH change, or approximately 0.02 units. That means that the resulting pH variability is as a result of processes such as biological production and respiration, mixing, sea ice melt and air-

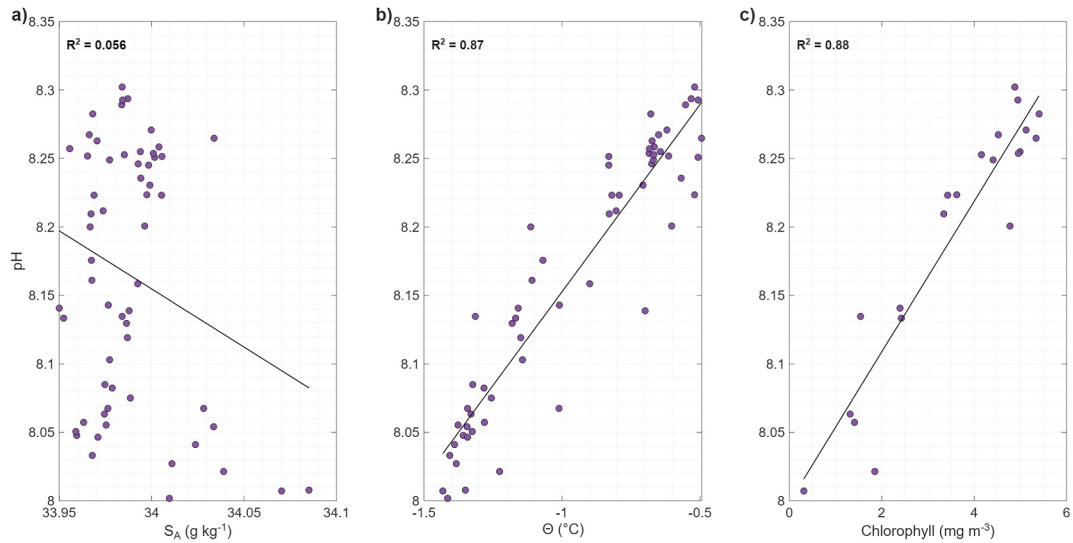


Figure 5. Upper ocean (less than 50 m depth) relationships between glider pH and (a) S_A, (b) Θ and (c) chlorophyll fluorescence with their corresponding R^2 value.

sea CO_2 exchange. The strong positive correlation between pH and chlorophyll fluorescence (Figure 5c) highlights the role of photosynthesis in driving upper ocean pH variation toward the end of the productive summer season. Previous research determined that iron plays a limiting role for phytoplankton in the ASP (Alderkamp et al., 2015), mostly toward the end of the summer (Twelves et al., 2021). As meltwater inputs are predicted to increase in the future (Gourmelen et al., 2017), the addition of important micronutrients and the glacial meltwater pump (St-Laurent et al., 2017; Twelves et al., 2021) could extend the duration of phytoplankton blooms. In the Amundsen Sea region the fate of the micronutrients is especially key for the ASP which is more iron limited than the adjacent Pine Island Polynya (Park et al., 2017). This indicates that carbon uptake in the ASP may increase, facilitated by primary production as glacial meltwater inputs increase. Kimura et al. (2017) suggest that the glacial meltwater pump enhances iron availability within the ASP. However, Twelves et al. (2021) argue that a stronger coastal current may limit the supply of iron from the glacial meltwater pump directly to the ASP, such that it therefore does not contribute to an increase in primary production in the ASP. Further earth system modeling efforts are needed to understand the effect that the glacial meltwater pump may have on carbonate chemistry in the future.

4.3. The Influence of the Coastal Current on Upper Ocean Carbonate Chemistry

To the east of DIS and Bear Island is an area often covered with fast ice (Nihashi & Ohshima, 2015; Ohshima et al., 2016) (Figure 1a). This fast ice influences the timing and distribution of sea ice formation and melt (Bett et al., 2020; Stammerjohn et al., 2015), thereby affecting the freshwater balance within the ASP. Its extent varies year to year (Fraser et al., 2020), but it was present year-round for one year prior to our campaign in 2022 (Figure 1a). Similar to Zheng et al. (2025), we propose that the coastal current transports unventilated water from under the fast ice westward toward DIS. This is supported by SADCP measurements in the upper 200 m that show a westward current emanating from the fast ice area and flowing along the DIS front (Figure 6a). Shipboard measurements show high surface water pCO_2 near the fast ice edge with values greater than 450 µatm (Figure 6b) along with a low dissolved O_2 concentration and an O_2 saturation of 70% (Figure 6c). The low oxygen saturation and high pCO_2 are typical of unventilated water in which remineralization has taken place (Bakker et al., 2008; Tynan et al., 2016). As water travels westward in the coastal current and is subject to air-sea gas exchange and biological productivity, it reaches O_2 saturation at approximately 111.5°W and CO_2 saturation (i.e., equilibrium of surface water pCO_2 with atmospheric pCO_2) by 111.0°W.

As water travels westwards with the coastal current from 111.0°W to DIS, biological CO_2 uptake further decreases pCO_2 (Figure 6b), increases O_2 saturation (Figure 6c) and the chlorophyll fluorescence (Figure 3d). The relatively low pH, Θ, S_A and chlorophyll concentration observed in the upper 50 m on the southern part of leg 4

21699291, 2026, 11, Downloaded from https://agupubs.onlinelibrary.wiley.com/doi/10.1029/2026JC024620 by British Antarctic Survey, Wiley Online Library on [13/11/2026]. See the Terms and Conditions (https://onlinelibrary.wiley.com/terms-and-conditions) on Wiley Online Library for rules of use; OA articles are governed by the applicable Creative Commons License

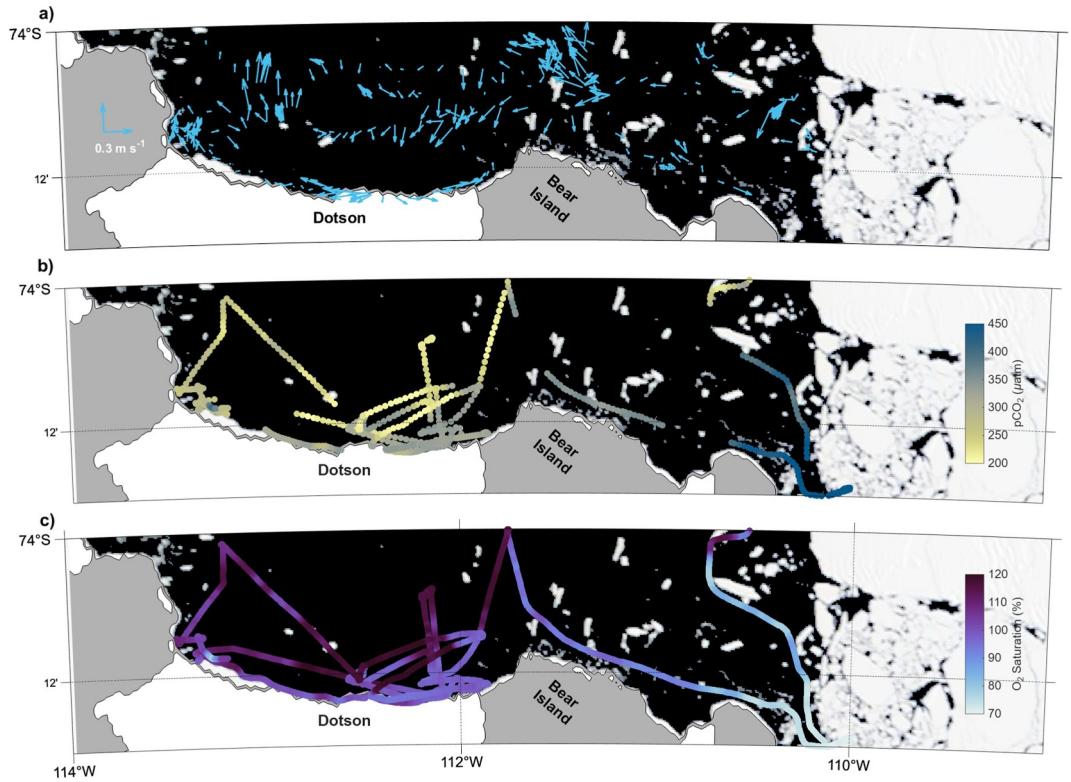


Figure 6. Current and surface water properties near Bear Island. (a) Current velocity (m s^{-1}) in the upper 200 m from the SADCP. (b) Shipboard surface water pCO_2 and (c) O_2 saturation. Satellite imagery of sea ice from Terra/MODIS on 21 January 2022.

(Figure 3) provide further evidence that water originating from the fast ice region has been transported westward and that the signal extends to the eastern side of DIS.

The glider crosses the coastal current in the southeastern corner of the glider box, at the eastern extent of legs 1, 5 and 6 on the eastern side of DIS. As the glider travels west, legs 1, 5 and 6 reach waters around 10 km north of the ice shelf front and are partly located north of the coastal current (Figures 3 and 6a). Therefore, some of the water encountered by the glider north of the center of DIS, especially on leg 5, likely represents surface water more typical of the open polynya, rather than of the coastal current. Chlorophyll fluorescence along leg 5, in particular, is similar to those along leg 3, with values of 4–6 mg m^{-3} (Figure 3d) but lower than the high values observed in the central polynya (around 12 mg m^{-3} (Alderkamp et al., 2015)). Along legs 1 and 6, some values of pH, Θ, S_A and chlorophyll resemble those on leg 3. Part of the differences between legs 1, 5 and 6 may be temporal as leg 1 was completed 10–11 days before leg 5 and the rest may be spatial as legs 1 and 6 are slightly further south than leg 5.

Mu et al. (2014) saw high surface pCO_2 (400–490 µatm) in front of DIS in December and early January, much greater than our values of 300–350 µatm (Figure 6b). Seasonal change could explain these differences as the water sampled by Mu et al. (2014) would have been only recently exposed to the atmosphere upon sea ice melt as the polynya opened, with less time for CO_2 outgassing and for biological CO_2 uptake than during our later survey.

The variability in pH demonstrates the close link between pH and biological carbon uptake in this region (Figure 5c). These small-scale differences in pH were resolved by the glider-LOC pH combination with comparisons made to continuous underway pCO_2 measurements (this study; Mu et al., 2014). Our results demonstrate the potential for this approach to capture spatial variability in coastal and polar environments.

21699291, 2026, 11, Downloaded from https://agupubs.onlinelibrary.wiley.com/doi/10.1029/2026JC024620 by British Antarctic Survey, Wiley Online Library on [13/11/2026]. See the Terms and Conditions (https://onlinelibrary.wiley.com/terms-and-conditions) on Wiley Online Library for rules of use; OA articles are governed by the applicable Creative Commons License

21699291, 2026, 11, Downloaded from https://agupubs.onlinelibrary.wiley.com/doi/10.1029/2026JC024620 by British Antarctic Survey, Wiley Online Library on [13/11/2026]. See the Terms and Conditions (https://onlinelibrary.wiley.com/terms-and-conditions) on Wiley Online Library for rules of use; OA articles are governed by the applicable Creative Commons License

4.4. The Potential of Lab-On-Chip Technology for Coastal Southern Ocean Observations

The results of this study demonstrate circumstances in which LOC pH measurements may be particularly valuable for autonomous ocean observations. The LOC sensor resolved spatial variability in pH which was important for identifying relatively small-scale carbonate chemistry gradients that would be impossible to resolve with discrete sampling alone. We suggest that this approach is particularly well suited to coastal and shelf environments where strong horizontal and vertical gradients are expected, particularly polar regions with sea ice and glacial meltwater. This is another benefit of utilizing stable LOC sensors, as deep samples for drift corrections are not required unlike for the electrochemical sensors used on profiling floats. The deep samples needed for drift corrections also limit the float use to further offshore than coastal regions. The observed bias between sensor and discrete samples of 0.01 suggest that the sensor is not yet sufficiently accurate to resolve long-term ocean acidification trends, for which an accuracy within 0.003 is needed (Newton et al., 2015) and instead is better suited to identifying regional dynamics and variability within coastal regions where an accuracy of better than 0.02 is required (Newton et al., 2015).

5. Conclusions

We present the first high-resolution, full-depth pH observations in front of the DIS in the Amundsen Sea using a spectrophotometric Lab-On-Chip pH sensor onboard a profiling Seaglider. These measurements highlight the contributions of both physical and biogeochemical processes to pH variability in front of DIS.

At depth, we show that mCDW entering the DIS cavity has a low pH and is altered through mixing with glacial meltwater, increasing pH by 0.03. Agreement between observed and derived pH demonstrates that the dilution by low DIC glacial meltwater is the primary driver of this pH change. However, as the outflow retains a strong mCDW signature, the pH in the meltwater-laden outflow remains 0.01 lower than that of surrounding water at the same density. This demonstrates that ice shelves with deep warm water intrusions may act to redistribute relatively low pH waters into the upper water column through the glacial meltwater pump.

In the upper ocean, pH variability is strongly correlated with chlorophyll, indicating that the biological CO_2 uptake during primary production has a dominant role. This study was carried out later in the summer season than previous investigations in this region that also found that primary productivity had a key role in pH and pCO_2 variability, highlighting its importance across the whole summer period. In contrast, within the coastal current, pH is relatively low, reflecting the properties of water that has emerged from beneath fast ice. The ability to resolve these small scale differences has been made possible by utilizing the LOC sensor-glider combination that increases the vertical and horizontal resolution of sampling in comparison to traditional ship-based sampling techniques.

As ice shelf melt rates are projected to increase over the coming decades, the processes identified are likely to become more significant in shaping regional carbonate chemistry and, more importantly, in regional ocean carbon uptake. Our study demonstrates the capability of LOC sensors on autonomous gliders to capture these dynamics at high-resolution, providing a novel approach for the monitoring of rapidly evolving polar regions. The measurements and findings presented in this study establish a baseline for assessing future changes in a region undergoing rapid ice shelf melt.

Conflict of Interest

The authors declare no conflicts of interest relevant to this study.

Availability Statement

The glider data set is publicly available on the British Oceanographic Database Centre at: https://doi.org/10.5285/35b7832c-2432-fb41-e063-7086abc0c610 (Heywood et al., 2025). The pH data set from SG579 is available separately at: https://doi.org/10.5285/33d1f143-47b5-a7d1-e063-7086abc03081 (Pickup, Hammermeister, et al., 2025). The underway pCO_2 measurements are available at: https://doi.org/10.25921/kyz6-z696 (Sweeney et al., 2023) and the underway O_2 measurements are published on Zenodo: https://doi.org/10.5281/zenodo.12647855 (Queste et al., 2024). Ship ADCP measurements are available in the Rolling Deck to Repository database: https://doi.org/10.7284/154856 (Wellner, 2022). Auxiliary data utilized in figures were BedMachinev3

21699291, 2026, 11, Downloaded from https://agupubs.onlinelibrary.wiley.com/doi/10.1029/2026JC024620 by British Antarctic Survey, Wiley Online Library on [13/11/2026]. See the Terms and Conditions (https://onlinelibrary.wiley.com/terms-and-conditions) on Wiley Online Library for rules of use; OA articles are governed by the applicable Creative Commons License

(Morlighem, 2022) which is available from the National Snow and Ice Centre Database. MODIS Terra true color corrected reflectance product images were obtained via NASA Worldview (https://worldview.earthdata.nasa.gov/).

Acknowledgments

Daisy Pickup's PhD research was supported by the Faculty of Science, UEA. This work is from the TARSAN project, a component of the International Thwaites Glacier Collaboration (ITGC). Support was received from the National Science Foundation (NSF: Grant 1941483—NSFGEO-NERC: ARTEMIS) and the Natural Environment Research Council (NERC: Grants NE/S006419/1 TARSAN and NE/W007045/1 ARTEMIS). Logistics were provided by the NSF (United States Antarctic Program) and the NERC (British Antarctic Survey). This is ITGC Contribution No. ITGC-168. We thank the United States Antarctic Program (USAP), including the captain, crew, and science team onboard the *R/V Nathaniel B. Palmer* 22-02 for field support. We also thank the UEA glider group for piloting the gliders during this campaign and the Ocean Technology and Engineering Group at the National Oceanography Centre for providing the Lab-On-Chip pH sensor. Additionally, we thank Hilde Oliver (Woods Hole Oceanographic Institution) for contributions to chlorophyll fluorescence processing.

References

Alderkamp, A.-C., van Dijken, G. L., Lowry, K. E., Connelly, T. L., Lagerström, M., Sherrell, R. M., et al. (2015). Fe availability drives phytoplankton photosynthesis rates during spring bloom in the Amundsen Sea Polynya, Antarctica. *Elementa: Science of the Anthropocene*, *3*, 000043. https://doi.org/10.12952/journal.elementa.000043

Arneborg, L., Wåhlin, A. K., Björk, G., Liljebladh, B., & Orsi, A. H. (2012). Persistent inflow of warm water onto the central Amundsen shelf. *Nature Geoscience*, *5*(12), 876–880. https://doi.org/10.1038/ngeo1644

Arrigo, K. R., Lowry, K. E., & van Dijken, G. L. (2012). Annual changes in sea ice and phytoplankton in polynyas of the Amundsen Sea, Antarctica. *Deep-Sea Research Part II Topical Studies in Oceanography*, *71–76*, 5–15. https://doi.org/10.1016/j.dsr2.2012.03.006

Arrigo, K. R., & van Dijken, G. L. (2003). Phytoplankton dynamics within 37 Antarctic coastal polynya systems. *Journal of Geophysical Research*, *108*(C8). https://doi.org/10.1029/2002jc001739

Assmann, K. M., Jenkins, A., Shoosmith, D. R., Walker, D. P., Jacobs, S. S., & Nicholls, K. W. (2013). Variability of Circumpolar Deep Water transport onto the Amundsen Sea Continental shelf through a shelf break trough. *Journal of Geophysical Research: Oceans*, *118*(12), 6603–6620. https://doi.org/10.1002/2013JC008871

Bakker, D. C. E., Hoppema, M., Schröder, M., Geibert, W., & de Baar, H. J. W. (2008). A rapid transition from ice covered CO_2 rich waters to a biologically mediated CO_2 sink in the eastern Weddell Gyre. *Biogeosciences*, *5*, 1373–1386. https://doi.org/10.5194/bg-5-1373-2008

Bett, D. T., Holland, P. R., Naveira Garabato, A. C., Jenkins, A., Dutrieux, P., Kimura, S., & Fleming, A. (2020). The impact of the Amundsen Sea freshwater balance on ocean melting of the West Antarctic Ice Sheet. *Journal of Geophysical Research: Oceans*, *125*(9), e2020JC016305. https://doi.org/10.1029/2020JC016305

Biddle, L. C., Loose, B., & Heywood, K. J. (2019). Upper ocean distribution of glacial meltwater in the Amundsen Sea, Antarctica. *Journal of Geophysical Research: Oceans*, *124*(10), 6854–6870. https://doi.org/10.1029/2019JC015133

Byrne, R. H., & Breland, J. A. (1989). High precision multiwavelength pH determinations in seawater using cresol red. *Deep-Sea Research, Part A: Oceanographic Research Papers*, *36*(5), 803–810. https://doi.org/10.1016/0198-0149(89)90152-0

Clayton, T. D., & Byrne, R. H. (1993). Spectrophotometric seawater pH measurements: Total hydrogen ion concentration scale calibration of m-cresol purple and at-sea results. *Deep Sea Research Part I: Oceanographic Research Papers*, *40*(10), 2115–2129. https://doi.org/10.1016/0967-0637(93)90048-8

Dickson, A. G., Sabine, C. L., Christian, J. R., & Organization, N. P. M. S. (2007). *Guide to best practices for ocean CO_2 measurements*. North Pacific Marine Science Organization.

Dinniman, M. S., St-Laurent, P., Arrigo, K. R., Hofmann, E. E., & van Dijken, G. L. (2020). Analysis of iron sources in Antarctic Continental shelf waters. *Journal of Geophysical Research: Oceans*, *125*(5), e2019JC015736. https://doi.org/10.1029/2019JC015736

Dotto, T. S., Sheehan, P. M. F., Zheng, Y., Hall, R. A., Damerell, G. M., & Heywood, K. J. (2025). Heterogeneous mixing processes observed in the Dotson Ice Shelf Outflow, Antarctica. *Journal of Geophysical Research: Oceans*, *130*(5), e2024JC022051. https://doi.org/10.1029/2024JC022051

Fraser, A. D., Massom, R. A., Ohshima, K. I., Willmes, S., Kappes, P. J., Cartwright, J., & Porter-Smith, R. (2020). High-resolution mapping of circum-Antarctic landfast sea ice distribution, 2000–2018. *Earth System Science Data*, *12*(4), 2987–2999. https://doi.org/10.5194/essd-12-2987-2020

Friedlingstein, P., O'Sullivan, M., Jones, M. W., Andrew, R. M., Bakker, D. C. E., Hauck, J., et al. (2026). Global carbon budget 2025. *Earth System Science Data Discussions*, *18*(5), 3211–3288. https://doi.org/10.5194/essd-18-3211-2026

Garau, B., Ruiz, S., Zhang, W. G., Pascual, A., Heslop, E., Kerfoot, J., & Tintoré, J. (2011). Thermal lag correction on Slocum CTD glider data. *Journal of Atmospheric and Oceanic Technology*, *28*(9), 1065–1071. https://doi.org/10.1175/JTECH-D-10-05030.1

Gourmelen, N., Goldberg, D. N., Snow, K., Henley, S. F., Bingham, R. G., Kimura, S., et al. (2017). Channelized melting drives thinning under a rapidly melting Antarctic ice shelf. *Geophysical Research Letters*, *44*(19), 9796–9804. https://doi.org/10.1002/2017GL074929

Green, R. E., Bower, A. S., & Lugo-Fernández, A. (2014). First autonomous bio-optical profiling float in the Gulf of Mexico reveals dynamic biogeochemistry in deep waters. *PLoS One*, *9*(7), 1–9. https://doi.org/10.1371/journal.pone.0101658

Ha, H. K., Wåhlin, A. K., Kim, T. W., Lee, S. H., Lee, J. H., Lee, H. J., et al. (2014). Circulation and modification of Warm Deep Water on the central Amundsen Shelf. *Journal of Physical Oceanography*, *44*(5), 1493–1501. https://doi.org/10.1175/JPO-D-13-0240.1

Hammermeister, E. M., Papadimitriou, S., Arundell, M., Ludgate, J., Schaap, A., Mowlem, M. C., et al. (2025). New capability in autonomous ocean carbon observations using the Autosub Long-Range AUV equipped with novel pH and total alkalinity sensors. *Environmental Science & Technology*, *59*(14), 7129–7144. https://doi.org/10.1021/acs.est.4c10139

Hammermeister, E. M., Wimart-Rousseau, C., Papadimitriou, S., Trucco-Pignata, P., Chaney, E., Templeton, R., et al. (2026). Coastal marine carbon and air-sea fluxes quantified from pH sensors on an extended AUV deployment. *Journal of Geophysical Research: Oceans*, *131*(8), e2025JC023213. https://doi.org/10.1029/2025JC023213

Heywood, K., Hall, R., Lee, G., Zheng, Y., Leadbitter, P., Rollo, C., et al. (2025). Temperature and salinity Seaglider observations in the Amundsen Sea, Antarctica, January - February 2022 [Dataset]. *NERC EDS British Oceanographic Data Centre NOC*. https://doi.org/10.5285/35b7832c-2432-fb41-e063-7086abc0c610

Hummon, J. M., & Firing, E. (2003). A direct comparison of two RDI shipboard ADCPs: A 75-kHz ocean surveyor and a 150-kHz narrow band. *Journal of Atmospheric and Oceanic Technology*, *20*(6), 872–888. https://doi.org/10.1175/1520-0426(2003)020(0872:ADCOTR2.0.CO;2

Jenkins, A. (1999). The impact of melting ice on ocean waters. *Journal of Physical Oceanography*, *29*(9), 2370–2381. https://doi.org/10.1175/1520-0485(1999)029(2370:TIOMIO2.0.CO;2

Jenkins, A., Shoosmith, D., Dutrieux, P., Jacobs, S., Kim, T. W., Lee, S. H., et al. (2018). West Antarctic Ice Sheet retreat in the Amundsen Sea driven by decadal oceanic variability. *Nature Geoscience*, *11*(10), 733–738. https://doi.org/10.1038/s41561-018-0207-4

Jiang, L. Q., Carter, B. R., Feely, R. A., Lauvset, S. K., & Olsen, A. (2019). Surface ocean pH and buffer capacity: Past, present and future. *Scientific Reports*, *9*(1), 18624. https://doi.org/10.1038/s41598-019-55039-4

Johnson, K. S., Jannasch, H. W., Coletti, L. J., Elrod, V. A., Martz, T. R., Takeshita, Y., et al. (2016). Deep-sea durafet: A pressure tolerant pH sensor designed for global sensor networks. *Analytical Chemistry*, *88*(6), 3249–3256. (PMID: 26890717). https://doi.org/10.1021/acs.analchem.5b04653

Johnson, K. S., Plant, J. N., Coletti, L. J., Jannasch, H. W., Sakamoto, C. M., Riser, S. C., et al. (2017). Biogeochemical sensor performance in the SOCCOM profiling float array. *Journal of Geophysical Research: Oceans*, *122*(8), 6416–6436. https://doi.org/10.1002/2017JC012838

Kim, C. S., Kim, T. W., Cho, K. H., Ha, H. K., Lee, S. H., Kim, H. C., & Lee, J. H. (2016). Variability of the Antarctic Coastal Current in the Amundsen Sea. *Estuarine, Coastal and Shelf Science*, *181*, 123–133. https://doi.org/10.1016/J.ECSS.2016.08.004

Kim, T.-W., Yang, H. W., Dutrieux, P., Wåhlin, A. K., Jenkins, A., Kim, Y. G., et al. (2021). Interannual variation of modified Circumpolar Deep Water in the Dotson-Getz trough, West Antarctica. *Journal of Geophysical Research: Oceans*, *126*(12), e2021JC017491. https://doi.org/10.1029/2021JC017491

Kimura, S., Jenkins, A., Regan, H., Holland, P. R., Assmann, K. M., Whitt, D. B., et al. (2017). Oceanographic controls on the variability of ice-shelf basal melting and circulation of glacial meltwater in the Amundsen Sea Embayment, Antarctica. *Journal of Geophysical Research: Oceans*, *122*(12), 10131–10155. https://doi.org/10.1002/2017JC012926

Kiuchi, M., Nomura, D., Hirano, D., Tamura, T., Hashida, G., Ushio, S., et al. (2021). The effect of basal melting of the Shirase Glacier Tongue on the CO_2 system in Lützow-Holm Bay, East Antarctica. *Journal of Geophysical Research: Biogeosciences*, *126*(5), e2020JG005762. https://doi.org/10.1029/2020JG005762

Legge, O. J., Bakker, D. C., Meredith, M. P., Venables, H. J., Brown, P. J., Jones, E. M., & Johnson, M. T. (2017). The seasonal cycle of carbonate system processes in Ryder Bay, West Antarctic Peninsula. *Deep-Sea Research Part II Topical Studies in Oceanography*, *139*, 167–180. https://doi.org/10.1016/j.dsr2.2016.11.006

Lewis, E., Wallace, D., & Allison, L. J. (1998). Program developed for CO_2 system calculations. https://doi.org/10.2172/639712

Lucio, A. J., Koopmans, D., Arundell, M., Loucaides, S., & Schaap, A. (2026). Obtaining accurate, high-frequency and long-term seawater pH data by using coupled lab-on-chip and optode sensing technologies. *Ocean Science*, *22*(3), 1609–1623. https://doi.org/10.5194/os-22-1609-2026

Macdonald, G. J., Ackley, S. F., Mestas-Nuñez, A. M., & Blanco-Cabanillas, A. (2023). Evolution of the dynamics, area, and ice production of the Amundsen Sea polynya, Antarctica, 2016-2021. *The Cryosphere*, *17*(2), 457–476. https://doi.org/10.5194/TC-17-457-2023

Mattsdotter Björk, M., Fransson, A., Torstensson, A., & Chierici, M. (2014). Ocean acidification state in western Antarctic surface waters: Controls and interannual variability. *Biogeosciences*, *11*(1), 57–73. https://doi.org/10.5194/bg-11-57-2014

Mazloff, M. R., Verdy, A., Gille, S. T., Johnson, K. S., Cornuelle, B. D., & Sarmiento, J. (2023). Southern Ocean acidification revealed by biogeochemical-argo floats. *Journal of Geophysical Research: Oceans*, *128*(5), e2022JC019530. https://doi.org/10.1029/2022JC019530

McDougall, T., Feistel, R., Millero, F., Jackett, D. R., Wright, D., King, B., et al. (2010). The international thermodynamic equation of seawater 2010 (TEOS-10): Calculation and use of thermodynamic properties.

Miles, T., Lee, S. H., Wåhlin, A., Ha, H. K., Kim, T. W., Assmann, K. M., & Schofield, O. (2016). Glider observations of the Dotson Ice Shelf outflow. *Deep Sea Research Part II: Topical Studies in Oceanography*, *123*, 16–29. https://doi.org/10.1016/J.DSR2.2015.08.008

Millero, F. J. (1995). Thermodynamics of the carbon dioxide system in the oceans. *Geochimica et Cosmochimica Acta*, *59*(4), 661–677. https://doi.org/10.1016/0016-7037(94)00354-O

Millero, F. J. (2007). The marine inorganic carbon cycle. *Chemical Reviews*, *107*(2), 308–341. https://doi.org/10.1021/cr0503557

Morlighem, M. (2022). MEaSUREs BedMachine Antarctica, version 3 [Dataset]. *NASA National Snow and Ice Data Center Distributed Active Archive Center*. https://doi.org/10.5067/FPSU0V1MWUB6

Mu, L., Stammerjohn, S. E., Lowry, K. E., & Yager, P. L. (2014). Spatial variability of surface pCO_2 and air-sea CO_2 flux in the Amundsen Sea Polynya, Antarctica. *Elementa: Science of the Anthropocene*, *3*, 000036. https://doi.org/10.12952/journal.elementa.000036

Nakayama, Y., Menemenlis, D., Schodlok, M., & Rignot, E. (2017). Amundsen and Bellingshausen Seas simulation with optimized ocean, sea ice, and thermodynamic ice shelf model parameters. *Journal of Geophysical Research: Oceans*, *122*(8), 6180–6195. https://doi.org/10.1002/2016JC012538

Naughten, K. A., Holland, P. R., & De Rydt, J. (2023). Unavoidable future increase in West Antarctic ice-shelf melting over the twenty-first century. *Nature Climate Change*, *13*(11), 1222–1228. https://doi.org/10.1038/s41558-023-01818-x

Naveira Garabato, A. C., Forryan, A., Dutrieux, P., Brannigan, L., Biddle, L. C., Heywood, K. J., et al. (2017). Vigorous lateral export of the meltwater outflow from beneath an Antarctic ice shelf. *Nature*, *542*(7640), 219–222. https://doi.org/10.1038/nature20825

Newton, J. A., Feely, R. A., Jewett, E. B., Williamson, P., & Mathis, J. (2015). (2nd ed.). Global ocean acidification observing network: Requirements and governance plan. GOA-ON.

Nihashi, S., & Ohshima, K. I. (2015). Circumpolar mapping of Antarctic coastal polynyas and landfast sea ice: Relationship and variability. *Journal of Climate*, *28*(9), 3650–3670. https://doi.org/10.1175/JCLI-D-14-00369.1

Ohshima, K. I., Nihashi, S., & Iwamoto, K. (2016). Global view of sea-ice production in polynyas and its linkage to dense/bottom water formation. *Geoscience Letters*, *3*, 1–14. https://doi.org/10.1186/S40562-016-0045-4/FIGURES/5

Orr, J. C., Epitalon, J.-M., Dickson, A. G., & Gattuso, J.-P. (2018). Routine uncertainty propagation for the marine carbon dioxide system. *Marine Chemistry*, *207*, 84–107. https://doi.org/10.1016/j.marchem.2018.10.006

Orr, J. C., Fabry, V. J., Aumont, O., Bopp, L., Doney, S. C., Feely, R. A., et al. (2005). Anthropogenic ocean acidification over the twenty-first century and its impact on calcifying organisms. *Nature*, *437*(7059), 681–686. https://doi.org/10.1038/nature04095

Padman, L., Fricker, H. A., Coleman, R., Howard, S., & Erofeeva, L. (2002). A new tide model for the Antarctic ice shelves and seas. *Annals of Glaciology*, *34*, 247–254. https://doi.org/10.3189/172756402781817752

Park, J., Kuzminov, F. I., Bailleul, B., Yang, E. J., Lee, S., Falkowski, P. G., & Gorbunov, M. Y. (2017). Light availability rather than Fe controls the magnitude of massive phytoplankton bloom in the Amundsen Sea polynyas, Antarctica. *Limnology and Oceanography*, *62*(5), 2260–2276. https://doi.org/10.1002/lno.10565

Pickup, D. D., Bakker, D. C. E., Heywood, K. J., Glassup, F., Hammermeister, E. M., Stammerjohn, S. E., et al. (2025). Cold lenses in the Amundsen Sea: Impacts of sea ice formation on subsurface pH and carbon. *Ocean Science*, *21*(6), 2727–2741. https://doi.org/10.5194/os-21-2727-2025

Pickup, D. D., Hammermeister, E. M., Loucaides, S., Lee, G. A., Bakker, D. C. E., Heywood, K. J., et al. (2025). pH measurements using a lab-on-chip sensor on a Seaglider in the Amundsen Sea, Antarctica, January - February 2022, version 2 [Dataset]. *NERC EDS British Oceanographic Data Centre NOC*. https://doi.org/10.5285/33d1f143-47b5-a7d1-e063-7086abc03081

Possenti, L., Humphreys, M. P., Bakker, D. C. E., Cobas-García, M., Fernand, L., Lee, G. A., et al. (2021). Air-sea gas fluxes and remineralization from a novel combination of pH and CO_2 sensors on a glider. *Frontiers in Marine Science*, *8*, 696772. https://doi.org/10.3389/fmars.2021.696772

Queste, B., Jacob, B., & du Plessis, M. (2024). Data used in the manuscript entitled "Turbulent heat flux dynamics along the Dotson and Getz ice-shelf fronts (Amundsen Sea, Antarctica)" [Dataset]. *Zenodo*. https://doi.org/10.5281/zenodo.12647855

Randall-Goodwin, E., Meredith, M. P., Jenkins, A., Yager, P. L., Sherrell, R. M., Abrahamsen, E. P., et al. (2015). Freshwater distributions and water mass structure in the Amundsen Sea Polynya region, Antarctica. *Elementa*, *3*, 000065. https://doi.org/10.12952/journal.elementa.000065

Reese, R., Albrecht, T., Mengel, M., Asay-Davis, X., & Winkelmann, R. (2018). Antarctic sub-shelf melt rates via PICO. *The Cryosphere*, *12*(6), 1969–1985. https://doi.org/10.5194/tc-12-1969-2018

21699291, 2026, 11, Downloaded from https://agupubs.onlinelibrary.wiley.com/doi/10.1029/2026JC024620 by British Antarctic Survey, Wiley Online Library on [13/11/2026]. See the Terms and Conditions (https://onlinelibrary.wiley.com/terms-and-conditions) on Wiley Online Library for rules of use; OA articles are governed by the applicable Creative Commons License

Sarmiento, J. L., Johnson, K. S., Arteaga, L. A., Bushinsky, S. M., Cullen, H. M., Gray, A. R., et al. (2023). The Southern Ocean carbon and climate observations and modeling (SOCCOM) project: A review. *Progress in Oceanography*, *219*, 103130. https://doi.org/10.1016/j.pocean.2023.103130

Sharp, J. D., Pierrot, D., Humphreys, M. P., Epitalon, J.-M., Orr, J. C., Lewis, E. R., & Wallace, D. W. (2023). CO2SYSv3 for MATLAB. *Zenodo*. https://doi.org/10.5281/zenodo.7552554

Sherrell, R. M., Lagerström, M. E., Forsch, K. O., Stammerjohn, S. E., & Yager, P. L. (2015). Dynamics of dissolved iron and other bioactive trace metals (Mn, Ni, Cu, Zn) in the Amundsen Sea Polynya, Antarctica. *Elementa*, *3*, 71. https://doi.org/10.12952/journal.elementa.000071

Stammerjohn, S. E., Maksym, T., Massom, R. A., Lowry, K. E., Arrigo, K. R., Yuan, X., et al. (2015). Seasonal sea ice changes in the Amundsen Sea, Antarctica, over the period of 1979–2014. *Elementa: Science of the Anthropocene*, *3*, 000055. https://doi.org/10.12952/journal.elementa.000055

St-Laurent, P., Yager, P. L., Sherrell, R. M., Stammerjohn, S. E., & Dinniman, M. S. (2017). Pathways and supply of dissolved iron in the Amundsen Sea (Antarctica). *Journal of Geophysical Research: Oceans*, *122*(9), 7135–7162. https://doi.org/10.1002/2017JC013162

Sweeney, C., Newberger, T., & Munro, D. R. (2023). Surface underway measurements of partial pressure of carbon dioxide (CO_2), sea surface temperature, sea surface salinity and barometric pressure during the *R/V Nathaniel B. Palmer* expeditions in the South Pacific Ocean, Drake Passage and Southern Ocean in 2022 (NCEI accession 0276572) [Dataset]. *NOAA National Centers for Environmental Information (NCEI)*. https://doi.org/10.25921/kyz6-z696

Tamura, T. P., Nomura, D., Hirano, D., Tamura, T., Kiuchi, M., Hashida, G., et al. (2023). Impacts of basal melting of the Totten Ice Shelf and biological productivity on marine biogeochemical components in Sabrina Coast, East Antarctica. *Global Biogeochemical Cycles*, *37*(9), e2022GB007510. https://doi.org/10.1029/2022GB007510

Thomalla, S. J., Moutier, W., Ryan-Keogh, T. J., Gregor, L., & Schütt, J. (2018). An optimized method for correcting fluorescence quenching using optical backscattering on autonomous platforms. *Limnology and Oceanography: Methods*, *16*(2), 132–144. https://doi.org/10.1002/lom3.10234

Tortell, P. D., Long, M. C., Payne, C. D., Alderkamp, A. C., Dutrieux, P., & Arrigo, K. R. (2012). Spatial distribution of pCO_2, $\Delta O_2/Ar$ and dimethylsulfide (DMS) in polynya waters and the sea ice zone of the Amundsen Sea, Antarctica. *Deep-Sea Research Part II Topical Studies in Oceanography*, *71–76*, 77–93. https://doi.org/10.1016/j.dsr2.2012.03.010

Twelves, A. G., Goldberg, D. N., Henley, S. F., Mazloff, M. R., & Jones, D. C. (2021). Self-shading and meltwater spreading control the transition from light to iron limitation in an Antarctic coastal polynya. *Journal of Geophysical Research: Oceans*, *126*(2), e2020JC016636. https://doi.org/10.1029/2020JC016636

Tynan, E., Clarke, J. S., Humphreys, M. P., Ribas-Ribas, M., Esposito, M., Rérolle, V. M., et al. (2016). Physical and biogeochemical controls on the variability in surface pH and calcium carbonate saturation states in the Atlantic sectors of the Arctic and Southern Oceans. *Deep-Sea Research Part II Topical Studies in Oceanography*, *127*, 7–27. https://doi.org/10.1016/j.dsr2.2016.01.001

Van Manen, M., Aoki, S., Brussaard, C. P. D., Conway, T. M., Eich, C., Gerringa, L. J. A., et al. (2022). The role of the Dotson Ice Shelf and Circumpolar Deep Water as driver and source of dissolved and particulate iron and manganese in the Amundsen Sea Polynya, Southern Ocean. *Marine Chemistry*, *246*, 104161. https://doi.org/10.1016/j.marchem.2022.104161

Walker, D. P., Jenkins, A., Assmann, K. M., Shoosmith, D. R., & Brandon, M. A. (2013). Oceanographic observations at the shelf break of the Amundsen Sea, Antarctica. *Journal of Geophysical Research: Oceans*, *118*(6), 2906–2918. https://doi.org/10.1002/jgrc.20212

Wellner, J. (2022). ADCP (Hawaii UHDAS) data as collected during the cruise NBP2202 [Dataset]. *Rolling Deck to Repository (R2R)*. https://doi.org/10.7284/154856

Wåhlin, A. K., Alley, K. E., Begeman, C., Ryvind, H., Yuan, X., Graham, A. G. C., et al. (2024). Swirls and scoops: Ice base melt revealed by multibeam imagery of an Antarctic ice shelf. *Science Advances*, *10*(31), eadn9188. https://doi.org/10.1126/sciadv.adn9188

Wåhlin, A. K., Kalén, O., Arneborg, L., Björk, G., Carvajal, G. K., Ha, H. K., et al. (2013). Variability of Warm Deep Water inflow in a submarine trough on the Amundsen Sea shelf. *Journal of Physical Oceanography*, *43*(10), 2054–2070. https://doi.org/10.1175/JPO-D-12-0157.1

Wåhlin, A. K., Yuan, X., Björk, G., & Nohr, C. (2010). Inflow of warm Circumpolar Deep Water in the central Amundsen shelf. *Journal of Physical Oceanography*, *40*(6), 1427–1434. https://doi.org/10.1175/2010JPO4431.1

Yager, P., Sherrell, R., Stammerjohn, S., Ducklow, H., Schofield, O., Ingall, E., et al. (2016). A carbon budget for the Amundsen Sea Polynya, Antarctica: Estimating net community production and export in a highly productive polar ecosystem. *Elementa: Science of the Anthropocene*, *4*, 000140. https://doi.org/10.12952/journal.elementa.000140

Yang, H. W., Kim, T. W., Dutrieux, P., Wåhlin, A. K., Jenkins, A., Ha, H. K., et al. (2022). Seasonal variability of ocean circulation near the Dotson Ice Shelf, Antarctica. *Nature Communications*, *13*(1), 1138. https://doi.org/10.1038/s41467-022-28751-5

Yin, T., Papadimitriou, S., Rérolle, V. M. C., Arundell, M., Cardwell, C. L., Walk, J., et al. (2021). A novel lab-on-chip spectrophotometric pH sensor for autonomous in situ seawater measurements to 6000 m depth on stationary and moving observing platforms. *Environmental Science & Technology*, *55*(21), 14968–14978. https://doi.org/10.1021/acs.est.1c03517

Zhang, X., Hu, L., & He, M.-X. (2009). Scattering by pure seawater: Effect of salinity. *Optics Express*, *17*(7), 5698–5710. https://doi.org/10.1364/OE.17.005698

Zheng, Y., Heywood, K., Webber, B., Stevens, D., Biddle, L., Boehme, L., & Loose, B. (2021). Winter seal-based observations reveal glacial meltwater surfacing in the southeastern Amundsen Sea. *Communications Earth & Environment*, *2*(1), 40. https://doi.org/10.1038/s43247-021-00111-z

Zheng, Y., Webber, B. G. M., Heywood, K. J., Stevens, D. P., Stammerjohn, S. E., & Hall, R. A. (2025). Upper-ocean processes and sea ice production in the southeastern Amundsen Sea polynya in austral autumn. *Journal of Physical Oceanography*, *55*(1), 43–58. https://doi.org/10.1175/JPO-D-24-0006.1

References From the Supporting Information

Dickson, A. G. (1990). Standard potential of the reaction: $AgCl(s) + 12H_2(g) = Ag(s) + HCl(aq)$, and the standard acidity constant of the ion HSO_4 in synthetic sea water from 273.15 to 318.15 K. *The Journal of Chemical Thermodynamics*, *22*(2), 113–127. https://doi.org/10.1016/0021-9614(90)90074-Z

Dickson, A. G., & Riley, J. P. (1979). The estimation of acid dissociation constants in sea-water media from potentiometric titrations with strong base. II. The dissociation of phosphoric acid. *Marine Chemistry*, *7*(2), 101–109. https://doi.org/10.1016/0304-4203(79)90002-1

21699291, 2026, 11, Downloaded from https://agupubs.onlinelibrary.wiley.com/doi/10.1029/2026JC024620 by British Antarctic Survey, Wiley Online Library on [13/11/2026]. See the Terms and Conditions (https://onlinelibrary.wiley.com/terms-and-conditions) on Wiley Online Library for rules of use; OA articles are governed by the applicable Creative Commons License

Millero, F. J., Pierrot, D., Lee, K., Wanninkhof, R., Feely, R., Sabine, C. L., et al. (2002). Dissociation constants for carbonic acid determined from field measurements. *Deep Sea Research Part I: Oceanographic Research Papers*, *49*(10), 1705–1723. https://doi.org/10.1016/S0967-0637(02)00093-6

Uppström, L. R. (1974). The boron/chlorinity ratio of deep-sea water from the Pacific Ocean. *Deep-Sea Research and Oceanographic Abstracts*, *21*(2), 161–162. https://doi.org/10.1016/0011-7471(74)90074-6

21699291, 2026, 11, Downloaded from https://agupubs.onlinelibrary.wiley.com/doi/10.1029/2026JC024620 by British Antarctic Survey, Wiley Online Library on [13/11/2026]. See the Terms and Conditions (https://onlinelibrary.wiley.com/terms-and-conditions) on Wiley Online Library for rules of use; OA articles are governed by the applicable Creative Commons License